Nano Energy 114 (2023) 108619

Contents lists available at ScienceDirect

Nano Energy

journal homepage: www.elsevier.com/locate/nanoen

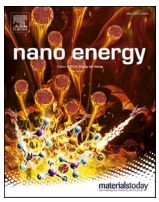

Spectral response regulation strategy by downshifting materials to improve efficiency of flexible perovskite solar cells

Xiaoguo Li [a,1], Fengming Xie [b,1], Saqib Rafique [a], Haoliang Wang [a], Liangliang Deng [a], Zejiao Shi [a], Yaxin Wang [a], Xin Zhang [a], Kai Liu [a], Yanyan Wang [a], Yiyi Pan [a], Fengcai Liu [a], Chongyuan Li [a], Tianxiang Hu [a], Jiao Wang [a], Anran Yu [a,*], Jianxin Tang [b,*], Yiqiang Zhan [a,*]

[a] Center of Micro-Nano System, School of Information Science and Technology, Fudan University, Shanghai 200433, China
[b] Jiangsu Key Laboratory for Carbon-Based Functional Materials & Devices, Institute of Functional Nano & Soft Materials (FUNSOM), Soochow University, Suzhou, Jiangsu 215123, China

ARTICLE INFO

Keywords:
Flexible perovskite solar cells
Downshifting
Spectral response
Stability

ABSTRACT

Polyethylene naphthalate (PEN) has been widely employed in highly desired flexible perovskite solar cells (F-PSCs) because of its better chemical stability and higher temperature tolerance. However, the naphthalene ring in the PEN induces poor transmittance in the ultraviolet (UV) region below 380 nm, which significantly lowers the power conversion efficiency (PCE) of F-PSCs. Here, a novel strategy is adopted by introducing UV–visible downshifting material before the PEN substrate to increase the spectral response under the UV region. The PCE of modified F-PSCs increases from 22.19 % to 22.81 % and retains the same stability as that of the control device. The optimized device shows improved photocurrent due to the enhanced spectral response in the UV region. Interestingly, the humidity resistance characteristic of the target device had also improved because of the hydrophobicity of downshifting materials. This novel strategy is distinguishable where downshifting material has been externally employed without altering the internal device architecture, which is also broadly applicable to other types of flexible solar cells.

1. Introduction

Flexible solar cells have emerged as promising candidates in photovoltaic technology owing to their lightweight and mechanical resilience which make them suitable to integrate into curved surfaces and convenient for storage and transportation [1–4]. Moreover, their potential can be explored in portable or wearable electronics [5], power generation textiles [6], building integrated photovoltaics and aerospace [7,8]. In this context, perovskite solar cells (PSCs) have made significant progress in recent years due to their outstanding properties, and the best-certified power conversion efficiency (PCE) of PSCs has reached to 25.7 % [9–12]. The PSCs can be fabricated using low-temperature, solution-process, and roll-to-roll manufacturing techniques, which are also suitable for flexible perovskite solar cells (F-PSCs). The certified PCE of F-PSCs has already surpassed the 23 % [13–15]. However, the performance and stability of the F-PSCs are not only affected by the quality of perovskite and charge transport layers but are also closely related to the optical and physical properties of flexible substrates.

Polyethylene terephthalate (PET) and polyethylene naphtholate (PEN) are commonly used as flexible substrates in F-PSCs. The structure of PET and PEN are shown in Fig. S1 while their properties are presented in Table S1. The double ring structure of the naphthalene group of the PEN can increase the thermal, chemical, mechanical, and barrier performance, which makes it superior to PET [16]. For instance, the glass-transition temperature (T_g) of PEN is 122 ℃, which is significantly higher than 80 ℃ of PET. Moreover, the working temperature of PEN can be up to 155 ℃ [17], which ensures good conductivity of the ITO based on the PEN substrate and makes it compatible with most of the perovskite preparation temperatures. More importantly, the PEN has a lower coefficient of thermal expansion [16], which leads to the reduced strain of the device and ultimately improves the performance of F-PSCs [18]. Owing to the aforementioned excellent properties of PEN, the F-PSCs based on PEN substrates can yield higher fill factor (FF), open-circuit voltage (V_{oc}) and ultimately reach higher PCE than

* Corresponding authors.
E-mail addresses: aryu@fudan.edu.cn (A. Yu), jxtang@suda.edu.cn (J. Tang), yqzhan@fudan.edu.cn (Y. Zhan).
[1] Xiaoguo Li and Fengming Xie equally contributed to this work.

https://doi.org/10.1016/j.nanoen.2023.108619
Received 30 March 2023; Received in revised form 29 May 2023; Accepted 16 June 2023
Available online 17 June 2023

PET-based devices [13]. Another advantage of PEN is its good gas barrier property, the oxygen and water permeability of PEN is three times lower than that of PET [19,20]. which is beneficial for long terms stability in real-world applications. Moreover, PEN substrates possess strong UV barrier properties, which can block sunlight below 380 nm, due to the presence of the bicyclic structure of the naphtholate ring [21]. It is well known that light-induced degradation, especially caused by the UV light of the solar spectrum, is a bottleneck in the long-term stability of PSCs [22], therefore, the device based on PEN substrates is stable under UV irradiation. However, the UV barrier properties of PEN will sacrifice the spectral energy in the range of 300–380 nm, consequently causing low photocurrent of solar cells. To overcome the drawback of the energy loss below 380 nm and keep the advantage of UV barrier property, a possible approach is to introduce downshifting materials, because of their ability of converting UV light to visible light, which can pass through the PEN substrate and can be absorbed by the perovskite. Previously, the downshifting materials has been introduced in PSCs to improve the performance of perovskite solar cells [23–25], especially improve the UV stability of TiO_2 electron transport layer (ETL) based PSCs due to the photocatalytic properties of TiO_2 [26]. Bella et al. reported Lumogen F Violet 570 as the downshifting layer on the front side of the PSCs device to prevent incident UV portions of the solar spectrum and improve the UV stability of TiO_2 based PSCs over 500 h under continuous illumination, and they found that the downshifting material can increase the photocurrent, leading to an increased PCE. However, it is difficult for the downshifting materials to fully absorb the UV light, therefore, part of the UV light still aggravate the interface of TiO_2 and perovskite [27]. Jin et al. reported the doping of downshifting material YVO_4:Eu^{3+},Bi^{3+} into the TiO_2 mesoporous layer to improve the UV stability and the photovoltaic response of the device, leading to a PCE enhancement from 16.3 % to 17.9 % [28]. Nevertheless, high conductivity requirement for downshifting materials when doping into the ETL is a bottleneck in their widespread usage. Additionally, downshifting materials possess lower EQE response for rigid device due to their higher transmittance in the rigid substrates than flexible substrate in the UV region. Although, the PEN based F-PSCs have much better UV stability than rigid PSCs, but the spectral energy loss caused by the PEN still remains unresolved.

In this work, for the first time, we developed a spectral response regulation method by combining thermally activated delayed fluorescence (TADF) material 3,5-di(9 H-carbazol-9-yl)− 2,6-bis(3,6-di-tert-butyl-9 H-carbazol-9-yl)benzonitrile (2Cz2tCzBn) with the PEN-based F-PSCs without altering the device structure. The 2Cz2tCzBn downshifting material possesses a wide absorption range at the UV region, a large absorption coefficient, and a high quantum yield, which has been introduced onto the front of the PEN substrate so that it could simultaneously absorb UV light, emit visible light, and compensate the energy loss between 300 and 380 nm caused by the absorption of PEN. Compared with the device without the downshifting material, which will be named the control device hereafter, the target device (with 2Cz2tCzBn layer) increased the photocurrent by 2.3 % and achieved a PCE of 22.81 % while retaining excellent UV stability. Moreover, it is noteworthy that the hydrophobicity of downshifting materials on the PEN substrate can prevent the permeability of humidity in the air into the perovskite layer, which is beneficial for environmental stability.

2. Results and discussion

To elucidate the weaker transmittance of PEN in the UV region, the transmittance of PEN and PET substrates were compared because it plays a critical role in photovoltaic performance. Fig. 1(a) shows the transmittance of PET/ITO and PEN/ITO substrates. It is clear that PET/ITO has high transmittance in the UV region that will contribute more photocurrent, however, it will also deteriorate the stability of the device when it is exposed to sunlight [29,30]. As previously reported, PEN is a useful UV filter that blocks UV light below 380 nm and significantly enhances the UV stability of F-PSCs [21]. On the other hand, the PEN-based device exhibited a low short-circuit current density (J_{sc}) of 22.97 mA/cm^2 as compared to 23.87 mA/cm^2 for the PET device. Consequently, the decreased J_{sc} leads to a lower PCE. The obvious decrease in J_{sc} and PCE is due to the low transmittance of PEN in the UV region as shown in Fig. 1(a). This can also be confirmed by the corresponding EQE spectra in Fig. 1(b). When PEN is used as a substrate, the corresponding device has extremely low EQE values in the UV region. In order to analyze the spectral energy loss in between 300 nm~400 nm, we prepared PSCs based on Glass/ITO, PET/ITO and PEN/ITO substrates and tested the corresponding EQE profiles, as shown in Fig. S2. The current density in the 300–400 nm range of these three devices were integrated according to the EQE, and the integrated current density were calculated to be 0.76 mA/cm^2, 0.75 mA/cm^2 and 0.33 mA/cm^2, respectively. It is clear that flexible devices based on PEN substrates have a current density loss of 0.42 mA/cm^2 before 400 nm compared to PET substrates.

Notably, downshifting materials can effectively reduce the energy loss that may occur due to the absorption of UV light by the PEN. TADF materials, owing to their ability of theoretical 100 % exciton harvesting for the singlet as well as triplet excitons utilizing efficient reverse intersystem crossing (RISC) process, are promising fluorescence emitters [31]. Here, the 2Cz2tCzBn is investigated as the downshifting layer because of its excellent solubility in common solvents, unique optical properties, and its chemical structure is shown in Fig. 2(a). Fig. 2(b) shows the absorption and emission spectra of 2Cz2tCzBn along with the EQE spectrum of control F-PSCs based on the PEN substrate. It can be seen that 2Cz2tCzBn has a wide absorption range from 280 nm to 450 nm with the absorption peak at 290 nm and 340 nm and the emission peak at 488 nm. In addition, photoluminescence quantum yield (PLQY) is also a key parameter of the fluorescence material, and the PLQY of 2Cz2tCzBn can reach up to 78 % in neat film [31]. Higher

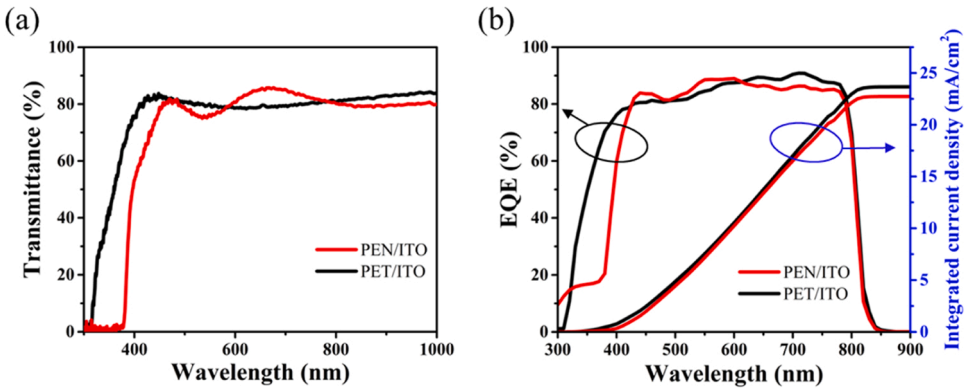

Fig. 1. (a) The transmittance spectra of PEN/ITO and PET/ITO; (b) the EQE spectra of flexible PSCs based on PEN and PET.

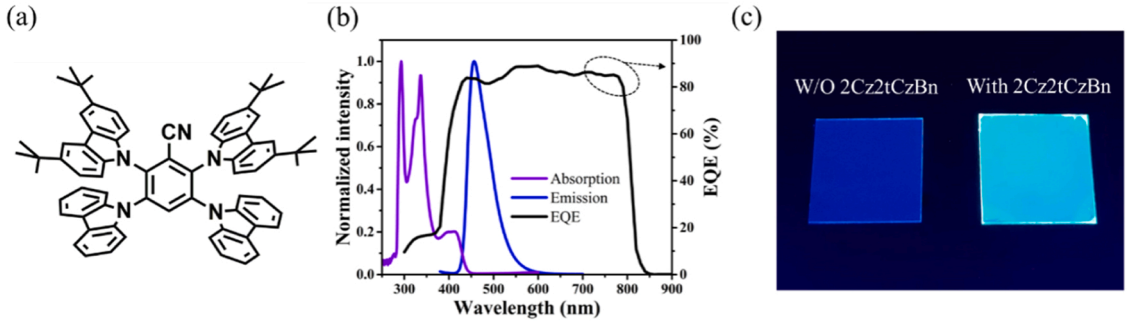

Fig. 2. (a) The molecule structure of 2Cz2tCzBn; (b) Emission and absorption spectra of 2Cz2tCzBn downshifting material and the EQE spectrum of PEN-based control F-PSCs; (c) Digital photographs of PEN with and without the downshifting layer when exposed to UV light.

PLQY can convert high-energy photons to low-energy photons more effectively. Moreover, it is important that downshifting material should have a large "Stokes shift" to avoid the fluorescence of downshifting materials absorbed by the PEN substrate. Fortunately, the distance between the absorption peak and the emission peak of 2Cz2tCzBn is more than 150 nm which depicts its long wavelength characteristics. Moreover, the optical properties of 2Cz2tCzBn are very much complementing the spectral response of F-PSCs devices on the pristine PEN substrate, as shown in Fig. 2(b). The absorption spectrum of 2Cz2tCzBn downshifting material has the strongest absorption in the UV region, while the F-PSCs based on PEN show very low EQE in this region. The EQE response of the perovskite absorption layer at the corresponding wavelength of the emission peak of 2Cz2tCzBn exceeds 80 % as shown in Fig. 2(b). All these factors make 2Cz2tCzBn downshifting material a worthy candidate to explore.

Fig. 2(c) is a real photograph of a substrate containing 2Cz2tCzBn downshifting material and a substrate without downshifting material under UV light irradiation. It can be seen that the downshifting material converts the UV light into brighter sky-blue light, while the UV light reflected by the substrate without the downshifting material appears dark blue, which indicates the capability of downshifting materials to effectively convert UV light into longer wavelength light.

To prove the role of downshifting materials in F-PSCs based on PEN substrate, we prepared devices with 2Cz2tCzBn/PEN/ITO/SnO_2/Perovskite/Spiro-OMeTAD/Au structure, as shown in Fig. 3(a). Fig. 3(b) shows the EQE spectra of devices with different concentrations of 2Cz2tCzBn. It is depicted in the EQE spectra that the spectral response has significantly improved in the UV region, which indicates that 2Cz2tCzBn can effectively convert the UV region (300–380 nm) of the solar spectrum into lower energy photons and thus it can be used by perovskite layer. Moreover, the concentration of 2Cz2tCzBn in DMF was also optimized. EQE of F-PSCs significantly increased in the range of 300–380 nm with the increase of 2Cz2tCzBn concentration from 0 mg/mL to 60 mg/mL, and the thickness of the downshifting layer are 59 nm, 109 nm, and 176 nm, respectively, when the concentration was 20 mg/mL, 40 mg/mL, and 60 mg/mL, as shown in Fig S3. To further analyze the effect of the downshifting layer on device performance the transmittance spectra was recorded, as shown in Fig S4. It is clear that the absorption of 2Cz2tCzBn was mainly located in the UV region, and the transmittance of the downshifting layers decreases when the thickness

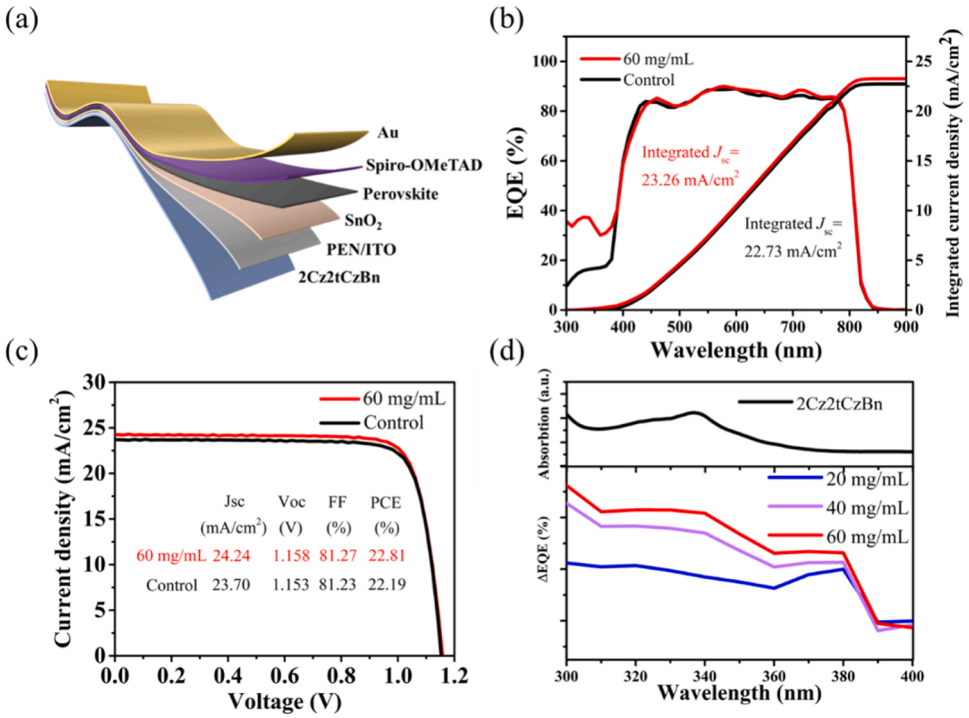

Fig. 3. (a) The structure of the flexible PSCs; (b) the EQE spectra of the F-PSCs with different concentrations of 2Cz2tCzBn; (c) the *J-V* curve of the champion devices with and without 2Cz2tCzBn layer; (d) the EQE subtractive spectra of different concentration of 2Cz2tCzBn minus the control device in the range between 300 nm∼400 nm.

increases. More importantly, as the increased concentration of 2Cz2tCzBn, the high transmittance typically above 98 %, indicates that the 2Cz2tCzBn have negligible effect on the perovskite absorption. It is worth noting that in the region of 300 nm~400 nm, the 2Cz2tCzBn have strong absorption, which makes the EQE significantly improved, but in the region of 400 nm~450 nm the absorption was weak, so the EQE was slightly decreased. However, due to the limitation of the solubility of the 2Cz2tCzBn downshifting material in the solvent, the solution tends to saturate at 60 mg/mL, and no further dissolution was possible. Therefore, the optimal concentration of the downshifting material in this work is 60 mg/mL. The integrated current density of the F-PSCs with an optimal concentration of downshifting materials and control devices are determined to be 23.26 mA/cm^2 and 22.73 mA/cm^2 respectively. The integrated current density in the range of 300–400 nm of the downshifting material-based device is 0.67 mA/cm^2, which indicates that the downshifting material can reduce 45 % energy loss in the UV region. Fig. 3(c) shows the *J-V* curves of the 2Cz2tCzBn (60 mg/mL) based target and pristine PEN-based control F-PSCs. It can be seen that the control device has achieved a PCE of 22.19 %, in which J_{sc} is 23.70 mA/cm^2, V_{oc} is 1.153 V, and FF is 81.23 %. While the PCE of 2Cz2tCzBn based target device increased to 22.81 %, and the J_{sc}, V_{oc}, and FF are 24.24 mA/cm^2, 1.158 V, and 81.27 %, respectively. While comparing these parameters, J_{sc} has the most obvious improvement followed by a slight improvement in V_{oc}. Fig. 3(d) shows the EQE spectra with different concentrations of 2Cz2tCzBn downshifting material minus the PEN pristine spectra (control device), and the trend of the curve is consistent with the absorption spectrum of the 2Cz2tCzBn, this indicates that the use of downshifting material before PEN has successfully converted UV light to visible light, which proves the effective role of the downshifting layer. Moreover, for comparison, PET-based devices without the 2Cz2tCzBn layer were also fabricated, the *J-V* curve and the corresponding EQE spectra of F-PSCs based on PET substrate are shown in Fig. S5 and S6, respectively. The 2Cz2tCzBn based target device outperformed both the pristine PEN and PET-based devices which proves the efficacy of the current work.

To further verify the role of the downshifting material, we theoretically estimated the EQE values in the UV region. In detail, the UV part of the incident light which is absorbed by the 2Cz2tCzBn molecule is denoted as A_{in}, and then the 2Cz2tCzBn molecule is excited with a certain quantum yield (η_{qy}) luminescence, a part of the emitted light is incident onto the perovskite absorption layer denoted as E_{pvsk}, and the other part is emitted into the air. The downshifting material 2Cz2tCzBn is an organic molecule, and its refractive index is about 1.73. At the interface between 2Cz2tCzBn film and the air, 50 % of the light emits to the air, and 50 % of the light flows into the layer of downshifting material. However, due to the total reflection, more than 50 % of the light from within the downshifting film will penetrate into the perovskite layer. This can be explained by the following relation also. According to the total reflection formula, the critical angle of total reflection can be calculated:

$$\theta = \arcsin\left(\frac{n_2}{n_1}\right) \tag{1}$$

Where, n_1 is the refractive index of the downshifting material, and n_2 is the refractive index of the air. Therefore, the critical angle of total reflection is 35.2°, which means that light with an incident angle greater than 35.2° will be reflected and transmitted through the downshifting layer and towards the perovskite layer. This has been depicted in Fig. S7 also. The blue color shows the part of the light that will transmit through the downshifting layer toward the perovskite layer, while the white color indicates the part of the light which has been transmitted into the air. To sum up, in the case of the total reflection, about 90.8 % of the light emitted from the downshifting material will be absorbed by the perovskite. The relevant calculation criteria are presented in Note S1 of the Supporting Information. The wavelength converted by downshifting material is λ and the EQE of the light (λ) converted into the current is denoted by EQE(λ). Therefore, EQE measured by devices with a downshifting layer can be expressed as [32]:

$$\mathrm{EQE}=A_{in}*\eta_{qy}*E_{pvsk}*\mathrm{EQE}(\lambda) \tag{2}$$

Based on the above considerations, the absorbance peak of 2Cz2tCzBn at 340 nm (A_{in}) is 65 % which is estimated from experimental data as shown in Fig. S8 of Supporting Information, the PLQY of 2Cz2tCzBn (η_{qy}) is 78 % and the 90.8 % of the emitted fluorescence enters into the perovskite (E_{pvsk}), while the EQE of perovskite at the emission peak (EQE(488)) is 85 % (Fig. 2(b)). It can be calculated from Eq. (2) that the maximum EQE with a downshifting layer in the near UV region is 39 %, which is consistent with the experimental results.

We further studied the reproducibility for different concentrations of 2Cz2tCzBn, and the statistical distributions of 20 devices of each concentration are provided in Fig. 4. There is an obvious increase in J_{sc} and PCE with the increasing concentration of 2Cz2tCzBn, however, a slight increase was observed in V_{oc}, while the FF almost remained unaffected. These results suggest that the PCE of F-PSCs can be improved by spectral regulation using downshifting materials.

Stability is an important indicator to analyze the commercial viability of devices. The UV stability of the F-PSCs devices based on PET/ITO, PEN/ITO, and 2Cz2tCzBn/PEN/ITO substrates were compared. During the aging test, the solar cells were stored in an N_2 glovebox and exposed to UV light (365 nm) with an intensity of 2 mW/cm^2, the PCE of the devices was measured during the aging process after regular intervals up to 560 h. As shown in Fig. 5(a), The PET/ITO devices suffered a 14 % PCE loss after 560 h of testing. In contrast, the PEN/ITO devices with and without downshifting layer filtering UV light maintained more than 95 % of initial PCE after the same aging time, showing superior UV stability than the PET device. These results demonstrate that the PEN substrate improves the UV stability of F-PSCs. While the use of 2Cz2tCzBn downshifting material maintains the stability of the PEN substrate.

More impotently, different from the rigid substrate, the polymer substrate has a certain gas permeability. Therefore, the long-term outdoor application of flexible substrate will lead to the gradual ingress of water and oxygen into the perovskite layer through these substrates, leading to the degradation of perovskite [33–35]. The common solution is to prepare a barrier layer on the back of the polymer substrate to prevent water vapor intrusion. However, it was anticipated that 2Cz2tCzBn is likely to prevent oxygen and water ingress into the inner layers owing to the hydrophobicity of the 2Cz2tCzBn. Therefore, we also characterized the water contact angle of 2Cz2tCzBn, as shown in Fig. 5 (b). After depositing 2Cz2tCzBn onto the back of PEN, the water contact angle of its surface increased from 59.13° to 85.60°, indicating that the downshifting material 2Cz2tCzBn has very good hydrophobicity. Hydrophobic surfaces will bring about two effects, firstly, the hydrophobic surface can effectively prevent air-borne water from directly contacting the PEN. On the other hand, in practical applications, hydrophobic surfaces also have a certain self-cleaning effect [27], that is, when it rains, rainwater will not be drained on the inclined surface, which can further prevent residual water from penetrating into the perovskite layer through PEN. To explore the influence of water vapor passing through PEN on perovskite materials, we first used Parylene to encapsulate perovskite films prepared on PET/ITO, PEN/ITO, 2Cz2tCzBn/PEN/ITO substrates, and put the encapsulated samples in a climate simulation box, with the relative humidity set at 80 % and the temperature at 25 ℃. Fig. 5(c) shows corresponding photographs which were taken after 0, 5, 10, and 30 days. After 5 days of accelerated aging in the climate simulation box, the attenuation of the perovskite edge area based on PET/ITO is obvious, and the other two samples have no obvious changes. After 10 days, the attenuation of perovskite-based on PET/ITO is more obvious, followed by the PEN where a slight change can also be observed, however, 2Cz2tCzBn/PEN/ITO remained conserved. This trend continued

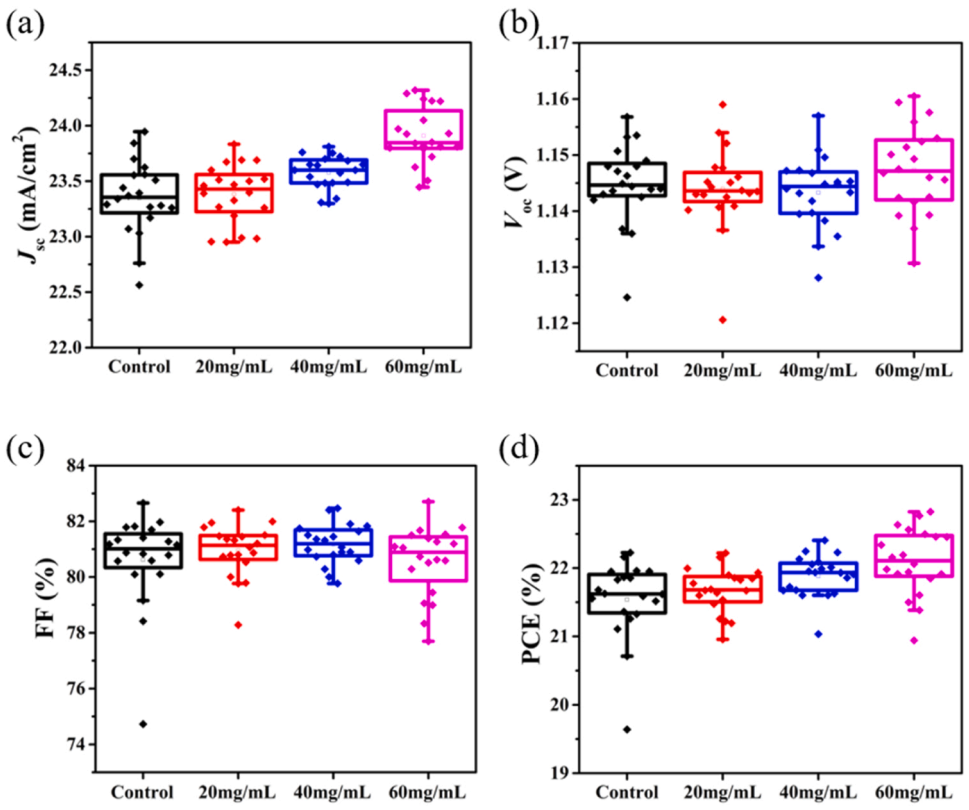

Fig. 4. Statistic distribution of photovoltaic parameters: (a) J_{sc}; (b) V_{oc}; (c) FF; (d) PCE.

even after 30 days and 2Cz2tCzBn/PEN/ITO was the least affected sample, while an obvious change can be observed in case of PET/ITO and PEN/ITO substrates. These results not only prove that PEN has a lower water vapor transmission rate than PET but also prove that the 2Cz2tCzBn downshifting material can successfully form a protective layer to prevent water vapor from directly penetrating into PEN and damaging the perovskite layer.

The flexibility of F-PSCs is critical for wearable power sources applications. To investigate the mechanical stability, the F-PSCs devices based on PEN and PEN-2Cz2tCzBn were bent at a radius of 5 mm continuously in the ambient condition with humidity of 30 %. The normalized PCE dependence with the bending cycles is shown in Fig. S9. After 1000 bending cycles, the PEN and PEN-2Cz2tCzBn devices retained 96.3 % and 95.8 % initial PCE, respectively. It can be seen that the 2Cz2tCzBn on the PEN substrate has a negligible effect on the mechanical stability of the device, due to the fact that 2Cz2tCzBn did not affect the crystallization and interface of the F-PSCs.

3. Conclusion

In summary, we integrated PEN with downshifting materials to improve the efficiency of F-PSCs. The downshifting material led to a more efficient spectral response in the UV region and to some extent remedies the energy loss incurred from absorbing the UV light of the PEN substrate. Compared with the control device which yielded a PCE of 22.19 %, the target device showed a PCE of 22.81 % and better UV, and humidity stability. This work highlights the role of spectral response regulation in improving the PCE of F-PSCs while maintaining their very good stability. It is believed, the current route can also be applied to other perovskite-based PSCs, and it paves the path to the realization of highly efficient and stable F-PSCs in the future. Moreover, the synergistic hybridization of the excellent UV absorption of downshifting materials, especially in the wavelength before 300 nm, and the very good radiation resistance of PEN substrate make the F-PSCs based on PEN substrate suitable for aerospace applications.

4. Experimental section

4.1. Materials

PEN/ITO (Peccell) was purchased from Advanced Election Technology Co. Ltd. A tin oxide (SnO_2) colloidal aqueous solution (15 % in H_2O) was obtained from Alfa Aesar. Dimethylformamide (DMF, anhydrous 99.8 %), Chlorobenzene, isopropanol (IPA, anhydrous 99.5 %), dimethyl sulfoxide (DMSO, anhydrous, 99.9 %), 4-tert-butylpyridine (4-TBP, 98 %), bis (trifluoromethylsulfonyl)-imide lithium salt (Li-TFSI, 99.99 %) and FK 209 (Co(III)-TFSI) were obtained from Sigma-Aldrich. Formamidinium iodide (FAI, 99.99 %), and methylammonium iodide (MAI, 99.99 %) have been purchased from Great Cell Energy and the Lead iodide (PbI_2, >99.8 %) were supplied from TCI. Methylammonium chloride (MACl, 99.5 %) and 2,2',7,7'-Tetrakis [N,N-di(4-methoxyphenyl)amino]− 9,9'-spirobifluorene (Spiro-OMeTAD, 99.5 %), Cyclohexylmethylammonium iodide (CHMAI, 99 %) were purchased from Xi'an Polymer Light Technology Corp. Polydimethylsiloxane (PDMS) was obtained from Dow. The Au was purchased from ZhongNuo Advanced Material (Beijing) Technology Co., Ltd. The 2Cz2tCzBn downshifting material was synthesized according to previous reports [31].

4.2. Device fabrication

The PEN/ITO substrates were sequentially cleaned with acetone and ethanol for 20 min followed by an N_2 blow-dry. The ITO side of the PEN substrate was then mounted onto the ultra-thin glass with double-sided tape to spin-coat 2Cz2tCzBn dissolved in DMF solution at the concentration of 20 mg/mL, 40 mg/mL, and 60 mg/mL, at the speed of 1000 rpm. The PEN substrate was then peeled off from the thin-glass slide. Another glass substrate was spin-coated with the PDMS to stick 2Cz2tCzBn/PEN/ITO onto the PDMS/glass substrate for further

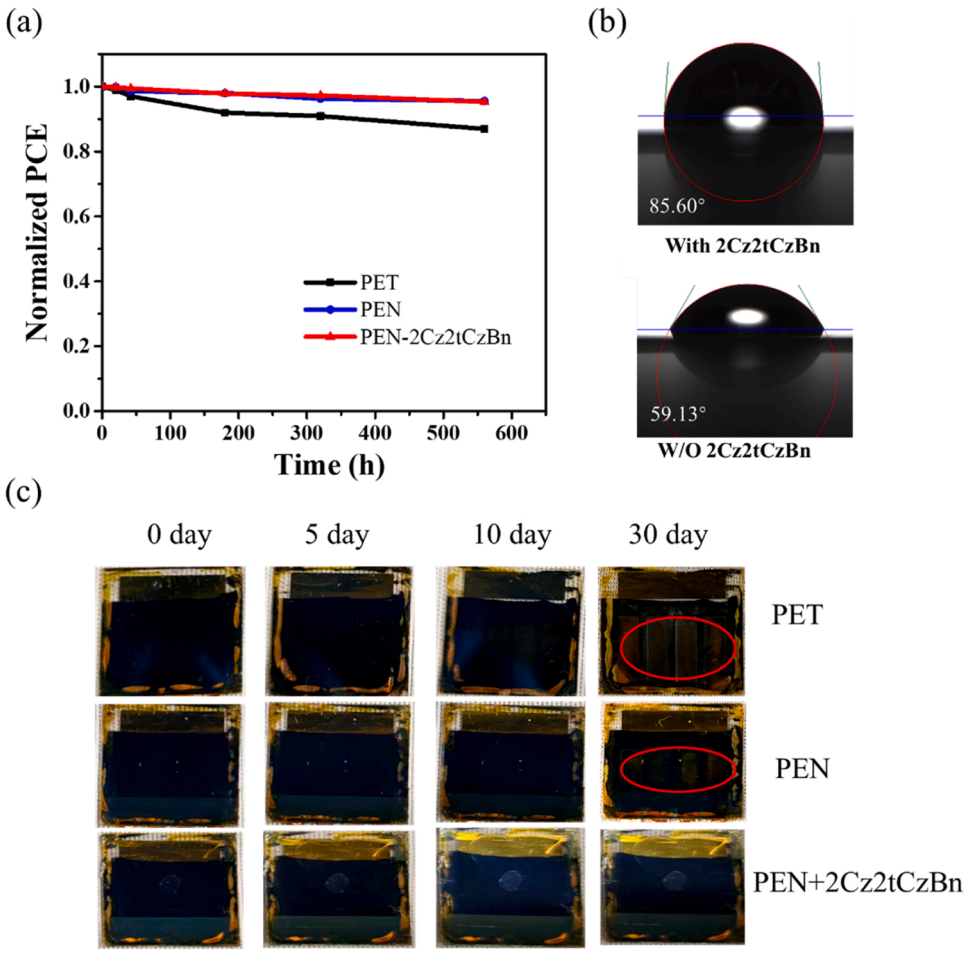

Fig. 5. (a) UV stability of F-PSCs with different substrates; (b) water contact angle of PEN substrate with and without 2Cz2tCzBn; (c) the device evolution of perovskite films based on different substrates under high humidity conditions.

deposition. The substrates were then treated with O_2 plasma for 5 min before depositing SnO_2 colloidal solution. The SnO_2 colloidal solution was first diluted 6 times by deionized water and then spin-coated at the speed of 3000 rpm for 30 s followed by annealing at 100 ℃ in the oven with a rough vacuum for 40 min. The perovskite solution was prepared using 695 mg of PbI_2 dissolved in 1 mL mixed solvent (DMF: DMSO, vol. ratio = 0.95: 0.05) and stirred for 3 h. The substrates were treated with UV-ozone for 15 min before coating PbI_2. The PbI_2 precursor was spin-coated on the SnO_2 film at 1500 rpm for 30 s, then the mixture solution of FAI: MACl: MAI (90 mg: 9 mg: 6 mg in 1 mL isopropanol) was spin-coated at 2000 rpm for 30 s followed by annealing at 150 °C for 20 min in ambient air. The perovskite surface was then treated by spin-coating CHMAI in isopropanol at the concentration of 6 mg/mL on the perovskite films at 6000 rpm for 30 s to passivate the surface defects. The hole-transport layer was deposited using Spiro-OMeTAD 72.3 mg/mL dissolved in 1 mL chlorobenzene with 29.0 μL of 4-tBP, 25.0 μL of FK209 (300 mg/mL in acetonitrile) and 18 μL Li-TFSI (520 mg/mL in acetonitrile), and spin-coated at 3000 rpm for 30 s. To complete the device fabrication, the Au electrode was thermally evaporated onto the Spiro-OMeTAD to obtain a thickness of 85 nm. Finally, the flexible PSCs were peeled off from the PDMS. For the stability test, F-PSCs were encapsulated using 5 μm parylene C and covered with UV-cured adhesive.

4.3. Characterization

The transmittance spectra were obtained using a filmetrics F20-UV thin-film analyzer. The photoluminescence measurement was carried out using a homemade system with a 405 nm excitation laser. External quantum efficiency (EQE) was measured using the QE-R system (Enlitech, Taiwan). Current density-voltage (*J-V*) curves of the flexible solar cells were recorded using a Keithley 2600 Source Meter at the 20 mV/s scan steps (from 1.2 V to −0.05 V for the reverse scan and from −0.05 V to 1.2 V for the forward scan) under AM 1.5 G (100 mW/cm^2) irradiation generated by sun simulator (Newport Sol3A ClassAAA). The intensity was calibrated by NREL Si reference solar cell, The active area of flexible perovskite solar cells was determined to be 0.072 cm^2 by the mask.

CRediT authorship contribution statement

Xiaoguo Li: fabricated and characterized the devices, analyzed data, and wrote the first draft. **Fengming Xie:** synthesized the downshifting materials, and characterized the properties of downshifting materials and revised and edited the manuscript. **Saqib Rafique:** revised and edited the manuscript and overall supervised the writing and editing of manuscript. **Haoliang Wang:** characterized the stability of the devices and analyzed data. **Liangliang Deng:** tested solar cell devices and analyzed data and revised the manuscript. **Zejiao Shi, Yaxin Wang, Xin Zhang:** characterized the devices, and analyzed the data. **Yanyan Wang, Yiyi Pan, Fengcai Liu:** tested solar cell devices and analyzed data**. Chongyuan Li, Jiao Wang:** revised and edited the manuscript. **Yiqiang Zhan:** provided funding for the project, proposed the idea, revised, and edited the manuscript plus supervised the project. **Jianxin Tang**: provided funding for the project and revised and edited the manuscript. **Anran Yu:** Performed calculations and revised and edited

the manuscript. In the final manuscript, all authors were involved in the analysis of the results and experimental phenomena.

Declaration of Competing Interest

The authors declare that they have no known competing financial interests or personal relationships that could have appeared to influence the work reported in this paper.

Data availability

Data will be made available on request.

Acknowledgements

This work was supported by the National Natural Science Foundation of China (Grant No. 62274040, 62274117).

Appendix A. Supporting information

Supplementary data associated with this article can be found in the online version at doi:10.1016/j.nanoen.2023.108619.

References

[1] R. Fan, Y. Huang, L. Wang, L. Li, G. Zheng, H. Zhou, Adv. Energy Mater. 6 (2016), 1600460.
[2] K. Zhang, K. Gao, R. Xia, Z. Wu, C. Sun, J. Cao, L. Qian, W. Li, S. Liu, F. Huang, X. Peng, L. Ding, H.-L. Yip, Y. Cao, High-performance polymer tandem Solar cells employing a new n-type conjugated polymer as an interconnecting layer, Adv. Mater. 28 (2016) 4817–4823.
[3] S. Jung, J. Lee, J. Seo, U. Kim, Y. Choi, H. Park, Development of annealing-free, solution-processable inverted organic solar cells with n-doped graphene electrodes using zinc oxide nanoparticles, Nano Lett. 18 (2018) 1337–1343.
[4] O.Y. Gong, G.S. Han, S. Lee, M.K. Seo, C. Sohn, G.W. Yoon, J. Jang, J.M. Lee, J. H. Choi, D.-K. Lee, S.B. Kang, M. Choi, N.-G. Park, D.H. Kim, H.S. Jung, Van der Waals force-assisted heat-transfer engineering for overcoming limited efficiency of flexible perovskite solar cells, ACS Energy Lett. 7 (2022) 2893–2903.
[5] Z. Wen, M.-H. Yeh, H. Guo, J. Wang, Y. Zi, W. Xu, J. Deng, L. Zhu, X. Wang, C. Hu, L. Zhu, X. Sun, Z.L. Wang, Self-powered textile for wearable electronics by hybridizing fiber-shaped nanogenerators, solar cells, and supercapacitors, Sci. Adv. 2 (2016), e1600097.
[6] L. Qiu, J. Deng, X. Lu, Z. Yang, H. Peng, Integrating perovskite solar cells into a flexible fiber, Angew. Chem. Int. Ed. 53 (2014) 10425–10428.
[7] A. Roy, A. Ghosh, S. Bhandari, S. Sundaram, T.K. Mallick, Perovskite solar cells for bipv application: a review, Buildings 10 (2020) 129.
[8] I. Cardinaletti, T. Vangerven, S. Nagels, R. Cornelissen, D. Schreurs, J. Hruby, J. Vodnik, D. Devisscher, J. Kesters, J. D'Haen, A. Franquet, V. Spampinato, T. Conard, W. Maes, W. Deferme, J.V. Manca, Organic and perovskite solar cells for space applications, Sol. Energy Mater. Sol. Cells 182 (2018) 121–127.
[9] X. Li, Z. Shi, F. Behrouznejad, M. Hatamvand, X. Zhang, Y. Wang, F. Liu, H. Wang, K. Liu, H. Dong, F. Mudasar, J. Wang, A. Yu, Y. Zhan, Highly efficient flexible perovskite solar cells with vacuum-assisted low-temperature annealed SnO2 electron transport layer, J. Energy Chem. 67 (2022) 1–7.
[10] F. Ruf, M.F. Aygüler, N. Giesbrecht, B. Rendenbach, A. Magin, P. Docampo, H. Kalt, M. Hetterich, APL Mater. 7 (2019), 031113.
[11] Q. Chen, N. De Marco, Y. Yang, T.-B. Song, C.-C. Chen, H. Zhao, Z. Hong, H. Zhou, Y. Yang, Under the spotlight: the organic–inorganic hybrid halide perovskite for optoelectronic applications, Nano Today 10 (2015) 355–396.
[12] B. Liu, Y. Wang, Y. Wu, Z. Liu, S. Bian, Y. Zhang, L. Liu, X. Zhuang, S. Liu, Z. Shi, X. Bai, L. Xu, D. Zhou, B. Dong, H. Song, Simultaneous bottom-up double-layer synergistic optimization by multifunctional fused-ring acceptor with electron-deficient core for stable planar perovskite solar cells with approaching 24% efficiency, Nano Energy 99 (2022), 107368.
[13] M. Li, J. Zhou, L. Tan, H. Li, Y. Liu, C. Jiang, Y. Ye, L. Ding, W. Tress, C. Yi, Multifunctional succinate additive for flexible perovskite solar cells with more than 23% power-conversion efficiency, Innovation 3 (2022), 100310.
[14] Y. Wu, G. Xu, J. Xi, Y. Shen, X. Wu, X. Tang, J. Ding, H. Yang, Q. Cheng, Z. Chen, Y. Li, Y. Li, [Protective role and mechanism of tubastatin A on renal and intestinal injuries after cardiopulmonary resuscitation in swine], Joule 7 (2023) 398–415.
[15] D. Gao, B. Li, Z. Li, X. Wu, S. Zhang, D. Zhao, X. Jiang, C. Zhang, Y. Wang, Z. Li, N. Li, S. Xiao, W.C.H. Choy, A.K. Jen, S. Yang, Z. Zhu, Highly efficient flexible perovskite solar cells through pentylammonium acetate modification with certified efficiency of 23.35, Adv. Mater. 35 (2023), e2206387.
[16] S.L. Sakellarides, Poly(ethylene naphthalate) (PEN), Encycl. Polym. Sci. Technol. (2004).
[17] M. Fonrodona, J. Escarré, F. Villar, D. Soler, J. Asensi, J. Bertomeu, J. Andreu, PEN as substrate for new solar cell technologies, Sol. Energy Mater. Sol. Cells 89 (2005) 37–47.
[18] L. Deng, X. Li, S. Rafique, Y. Wang, Y. Wang, K. Liu, F. Liu, Y. Pan, X. Yue, J. Wang, J. Tang, Y. Yang, H. Wang, Z. Shi, C. Li, Y. Qin, A. Yu, Y. Zhan, Strain release and defect passivation in formamidinium-dominated perovskite via a novel in-plane thermal gradient assisted crystallization strategy, ACS Appl. Mater. Interfaces 14 (2022) 52007–52016.
[19] H. Nörenberg, M.J. Percy, in, 2006.
[20] Y.H.Z.D.G.Y. Ren Xiaohe, Petrochem. Technol. 50 (2021) 616–621.
[21] L.G. Molokanova, Y.K. Kochnev, A.N. Nechaev, S.N. Chukova, P.Y. Apel, Effect of ultraviolet radiation on polyethylene naphthalate films irradiated with high-energy heavy ions, High. Energy Chem. 51 (2017) 182–188.
[22] W. Li, W. Zhang, S. Van Reenen, R.J. Sutton, J. Fan, A.A. Haghighirad, M. B. Johnston, L. Wang, H.J. Snaith, Energy Environ. Sci. 9 (2016) 490–498.
[23] Q. Wang, X. Zhang, Z. Jin, J. Zhang, Z. Gao, Y. Li, S.F. Liu, Energy-down-shift CsPbCl3:Mn quantum dots for boosting the efficiency and stability of perovskite solar cells, ACS Energy Lett. 2 (2017) 1479–1486.
[24] B. Wang, B. Li, T. Shen, M. Li, J. Tian, ZnSe quantum dots downshifting layer for perovskite solar cells, J. Energy Chem. 27 (2018) 736–741.
[25] B. Liu, Y. Wang, Y. Wu, B. Dong, H. Song, J. Mater. Sci. Technol. 140 (2023) 33–57.
[26] M.M. Tavakoli, F. Giordano, S.M. Zakeeruddin, M. Grätzel, Mesoscopic oxide double layer as electron specific contact for highly efficient and UV stable perovskite photovoltaics, Nano Lett. 18 (2018) 2428–2434.
[27] F. Bella, G. Griffini, J.-P. Correa-Baena, G. Saracco, M. Grätzel, A. Hagfeldt, S. Turri, C. Gerbaldi, Improving efficiency and stability of perovskite solar cells with photocurable fluoropolymers, Science 354 (2016) 203–206.
[28] J. Jin, H. Li, C. Chen, B. Zhang, W. Bi, Z. Song, L. Xu, B. Dong, H. Song, Q. Dai, Improving efficiency and light stability of perovskite solar cells by incorporating YVO4:Eu3+, Bi3+nanophosphor into the mesoporous TiO2 layer, ACS Appl. Energy Mater. 1 (2018) 2096–2102.
[29] M. Ouafi, B. Jaber, L. Atourki, R. Bekkari, L. Laânab, Improving UV stability of MAPbI3 perovskite thin films by bromide incorporation, J. Alloy. Compd. 746 (2018) 391–398.
[30] K. Deng, Q. Chen, Y. Shen, L. Li, Improving UV stability of perovskite solar cells without sacrificing efficiency through light trapping regulated spectral modification, Sci. Bull. 66 (2021) 2362–2368.
[31] F.-M. Xie, Z.-D. An, M. Xie, Y.-Q. Li, G.-H. Zhang, S.-J. Zou, L. Chen, J.-D. Chen, T. Cheng, J.-X. Tang, tert-Butyl substituted hetero-donor TADF compounds for efficient solution-processed non-doped blue OLEDs, J. Mater. Chem. C 8 (2020) 5769–5776.
[32] L.H. Slooff, R. Kinderman, A.R. Burgers, N.J. Bakker, J.A.M. van Roosmalen, A. Büchtemann, R. Danz, M. Schleusener, Efficiency enhancement of solar cells by application of a polymer coating containing a luminescent dye, J. Sol. Energy Eng. 129 (2006) 272–276.
[33] J. Yang, Z. Yuan, X. Liu, S. Braun, Y. Li, J. Tang, F. Gao, C. Duan, M. Fahlman, Q. Bao, Oxygen- and water-induced energetics degradation in organometal halide perovskites, ACS Appl. Mater. Interfaces 10 (2018) 16225–16230.
[34] K. Kwak, E. Lim, N. Ahn, J. Heo, K. Bang, S.K. Kim, M. Choi, An atomistic mechanism for the degradation of perovskite solar cells by trapped charge, Nanoscale 11 (2019) 11369–11378.
[35] G. Wu, X. Dong, J. Xiu, Y. Yu, M. Gu, T.B. Tang, Z. Zuo, Y. Liu, G. Cui, Water and oxygen co-induced microstructure relaxation and evolution in CH(3)NH(3)PbI(3), Phys. Chem. Chem. Phys. 23 (2021) 17242–17247.